

COMPOSITE BEHAVIOR OF SEGMENTAL PRECAST ULTRA-HIGH PERFORMANCE FIBER-REINFORCED CONCRETE SLABS AND FRP GIRDERS

Hai Nguyen, PhD, Research Associate, Nick J. Rahall, II Appalachian Transportation Institute, Marshall University, Huntington, West Virginia, USA

Hiroshi Mutsuyoshi, PhD, PE, Professor, Department of Civil and Environmental Engineering, Saitama University, Saitama, Japan

Wael Zatar, PhD, Dean and Professor, College of Information Technology and Engineering, Marshall University, Huntington, West Virginia, USA

ABSTRACT

This paper presents findings on the flexural behavior of composite girders consisting of precast Ultra-High Performance Fiber-Reinforced Concrete (UHPFRC) slabs and Fiber-Reinforced Polymer (FRP) I-girders. Seven large-scale composite girders and two control girder specimens were tested monotonically under four-point flexural loading. Two series of the FRP-UHPFRC composite girders were prepared. H-series girders included hybrid carbon/glass FRP (HFRP) I-girders topped with either full-length precast UHPFRC slabs or segmental counterparts. G-series girders composed of segmental UHPFRC slabs rested on glass-fiber-reinforced polymer (GFRP) I-girders. Twelve precast UHPFRC segments were used in each slab of the segmental composite girders. Either epoxy or high-strength mortar connections were used to connect the precast UHPFRC segments. The test results showed that the mortar-connected girder exhibited more ductile behavior than the epoxy-connected girder. The G-series girder with an 8 mm (0.315 in.) thick GFRP plate externally bonded to the soffit of the GFRP I-girder exhibited pseudo-ductile behavior. All the composite girders demonstrated significant improvements in strength and stiffness as compared to the control FRP I-girders without the UHPFRC slabs. The FRP-UHPFRC composite girders were shown to provide a promising and sustainable solution for accelerated bridge construction.

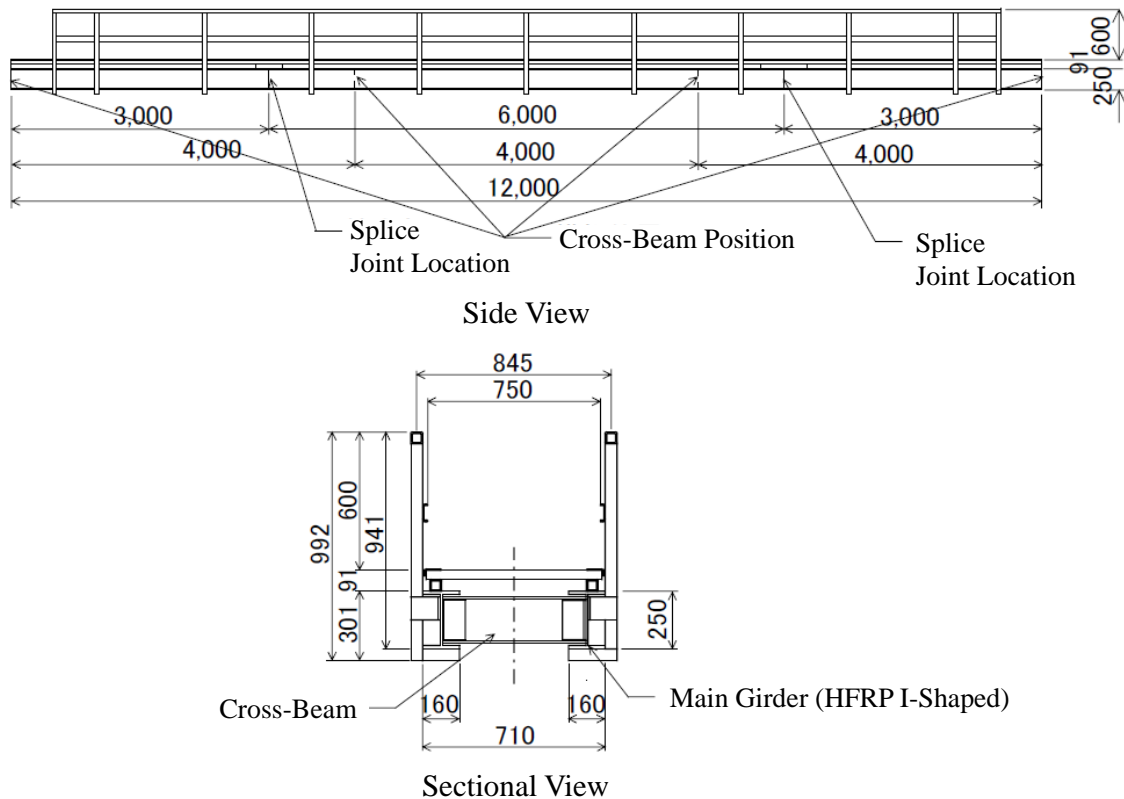
Keywords: Fiber-Reinforced Polymer I-Girder, Ultra-High Performance Fiber-Reinforced Concrete Slab, Full-Length Precast Slab, Segmental Precast Slabs, Flexural stiffness, Ultimate strength.

INTRODUCTION

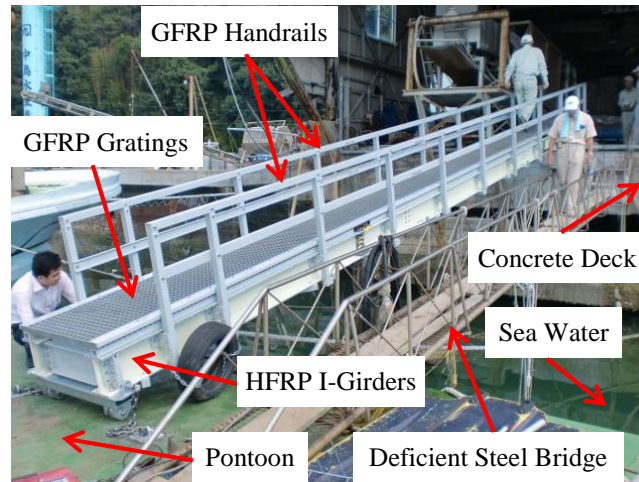
Of the 607,380 existing bridges in the United States, 24.9% have been deemed structurally deficient and/or functionally obsolete. The Federal Highway Administration (FHWA) estimates that federal, state, and local governments would need to invest \$20.5 billion annually to eliminate the nation's bridge backlog by 2028 (ASCE 2013). It is therefore important to find material and technology solutions to effectively address these deteriorating bridges. Fiber-Reinforced Polymer (FRP) materials are very attractive in the construction industry due to their high strength-to-weight ratio, low maintenance cost, and corrosion resistance. The authors have developed hybrid FRP (HFRP) I-girders for bridge applications in which the use of carbon-fiber-reinforced polymer (CFRP) and glass-fiber-reinforced polymer (GFRP) in a girder section with a specific ratio of flange to web width was optimal (Nguyen et al. 2010). The top and bottom flanges of the HFRP I-girder included multiple laminae of CFRP and GFRP. CFRP has higher tensile strength and stiffness than GFRP, but it is relatively expensive. The web of the HFRP I-girder was made of GFRP laminae due to its lower stress demand (than that on the flanges) and lower cost. As a result, the HFRP I-girder utilizes the advantages of both CFRP and GFRP. The HFRP girders can potentially be used in aggressive environments and in accelerated bridge construction due to their low weight and corrosion-free characteristics.

The authors reported that the design of the HFRP I-girders was governed by deflection rather than strength limitations (Nguyen et al. 2010). This was due to the low elastic modulus of the FRP materials (as compared to steel alternatives). Although the HFRP girders may have lower stiffness and strength as compared to steel bridge girders, they can be used with FRP decks to form pedestrian bridges. Figure 1 shows the successful application of the HFRP I-girders to construct a pedestrian bridge in Kure city, Hiroshima prefecture, Japan, in 2011. The bridge was used to replace an existing corroded steel bridge (Fig. 1b). The replacement bridge is composed of a GFRP grating deck rested on two HFRP I-girders. It has a single span with a total length of 12 m (39.34 ft) and an effective width of 0.75 m (2.46 ft). The bridge is simply supported between a concrete deck and a pontoon in a fishery harbor (Fig. 1b). The bridge's proximity to the ocean subjects it to a highly corrosive environment. Since completion, its condition has been periodically assessed by visual inspection and by the monitoring of strain gauge readings attached to the HFRP I-girders.

For vehicular bridges, it is necessary to provide a concrete slab on top of the HFRP I-girder to carry the compression force, thus reducing stresses and deflection/deformation of the HFRP girder and preventing delamination failure and buckling of the HFRP compression flange. Extensive studies have been carried out on the behavior of FRP-concrete used in bridges and buildings (Bakeri and Sunder 1990, Deskovic et al. 1995, Fam and Rizkalla 2002, Correia et al. 2007, and Keller et al. 2007). These studies showed the feasibility of using a FRP-concrete girder system for infrastructure applications. Most of these studies, however, focused on the use of normal strength concrete (NSC). The use of NSC requires a larger slab cross-sectional area to obtain tensile failure for FRP girder. This study focuses on the flexural behavior of the precast Ultra-High Performance Fiber-Reinforced Concrete (UHPFRC) slabs rested on the FRP I-girders. UHPFRC is a durable material (Sakai and Noguchi 2013) and it has high ductility in both tension and compression due to the crack-bridging effect of the high-strength steel fibers. The fibers assist in resisting shrinkage and temperature effects, resulting in reduced slab thickness and weight of the composite girder.



(a) Details of HFRP pedestrian bridge (dimensions in millimeters)



(b) Completion of HFRP pedestrian bridge connecting a pontoon and a concrete deck
 Fig. 1 First HFRP pedestrian bridge using HFRP I-girders in fishery harbor in Kure, Hiroshima, Japan (2011)

The authors investigated the flexural behavior of the HFRP-UHPFRC composite girders using a full-length precast UHPFRC slab (Mutsuyoshi et al. 2011, Nguyen et al. 2013, and Nguyen et al. 2015). Compared to control HFRP girders without topping slabs, the authors determined HFRP-UHPFRC composite girders could provide significant flexural strength and stiffness improvements. The full-length slabs were cast and cured at a precast plant with better quality control than cast-in-place concrete. Generally speaking, slender precast slabs – with adequate supports – can be safely transported to a construction site. However, the slabs can have a high slenderness ratio, as the UHPFRC is supposed to be able to reach a compressive strength of up to 800 N/mm^2 (116,110 psi) (Sugano et al. 2007). Transportation of these slabs might present a challenge as their slenderness ratio might result in unwarranted cracks and/or deflections.

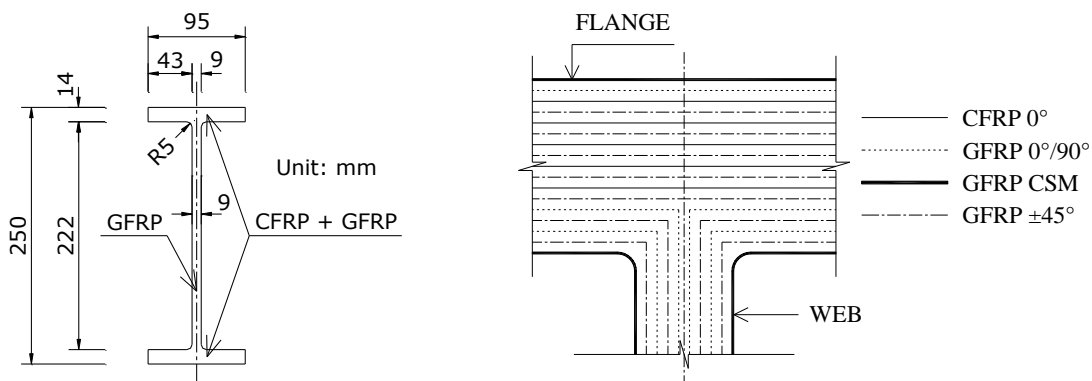
The purpose of this study is to evaluate the flexural behavior of segmental precast UHPFRC slabs rested on FRP I-girders. The precast segments could have smaller slenderness ratios than the full-length counterparts and they could thus be easily transported to the construction sites without developing significant deformations or cracks. The research also investigates the connections between precast segments using either epoxy adhesive or high-strength mortar. The experimental program described herein is a part of a comprehensive experimental program that is focused on developing a sustainable girder system for bridge applications.

LARGE-SCALE FLEXURAL TESTING OF PRECAST FRP-UHPFRC COMPOSITE GIRDERS

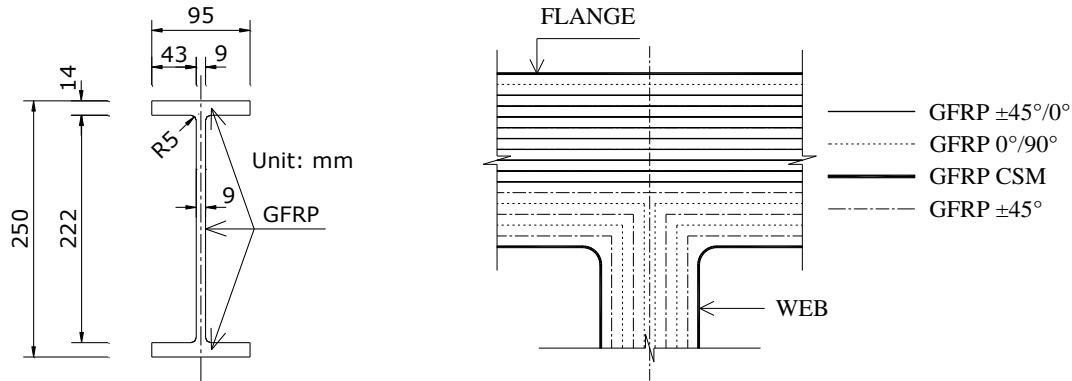
MATERIALS

GFRP and HFRP I-Girders

The pultruded HFRP and GFRP I-girders were used in large-scale flexural tests of composite girders (Fig. 2). The HFRP/GFRP I-girders were connected to the precast UHPFRC slabs by epoxy adhesive and high corrosion resistant steel (HCRS) headed bolt shear connectors. The flanges of the HFRP I-girders were composed of CFRP and GFRP, while those of the GFRP girders were made entirely of GFRP. Unidirectional carbon fibers (fibers were oriented at zero degree to the longitudinal direction) were used in the flanges of the HFRP girders. Bi-directional glass fiber fabric (fibers were oriented at $0^\circ/90^\circ$, $\pm 45^\circ$, or $\pm 45^\circ/0^\circ$ directions) and glass fiber continuous strand mat (fibers were randomly oriented) were used in the flanges and the web of both the HFRP and GFRP I-girders. The overall height of the HFRP/GFRP girders was 250 mm (9.84 in.) and the flange width was 95 mm (3.74 in.). The flange thickness was 14 mm (0.55 in.) and the web thickness was 9 mm (0.35 in.). Details of cross-sectional dimensions, layer compositions, and laminate stacking sequence of the HFRP/GFRP I-girders are shown in Fig. 2. Mechanical properties of FRP laminae in the flanges and web of the HFRP/GFRP girders as well as the equivalent mechanical properties of the flanges and web of the HFRP/GFRP I-girders obtained from material tests are listed in Table 1.



(a) Cross-sectional dimensions, layer compositions, and laminate stacking sequence of HFRP I-girder



(b) Cross-sectional dimensions, layer compositions, and laminate stacking sequence of GFRP I-girder

Fig. 2 Details of HFRP and GFRP I-girders (dimensions in millimeters)

Table 1 Material Properties of HFRP/GFRP I-Girders

<i>Mechanical Properties of FRP Laminae in Flanges and Web of HFRP/GFRP I-Girders</i>									
Parameters	Notation	HFRP I-Girder				GFRP I-Girder			
		CFRP 0°	GFRP 0/90°	GFRP ±45°	GFRP CSM	GFRP ±45°/0°	GFRP 0/90°	GFRP ±45°	GFRP CSM
Volume Fraction	V_f , %	55	53	53	25	53	53	53	25
Volume Content	Flanges, %	33	17	41	9	33	17	41	9
	Web, %	0	43	43	14	0	43	43	14
Young's Modulus	E_{11} , GPa (ksi)	128.1 (18,580)	25.9 (3,760)	11.1 (1,610)	11.1 (1,610)	-	25.9 (3,760)	11.1 (1,610)	11.1 (1,610)
	E_{22} , GPa (ksi)	14.9 (2,160)	25.9 (3,760)	11.1 (1,610)	11.1 (1,610)	-	25.9 (3,760)	11.1 (1,610)	11.1 (1,610)
Shear Modulus	G_{12} , GPa (ksi)	5.5 (800)	4.4 (640)	10.9 (1,580)	4.2 (610)	-	4.4 (640)	10.9 (1,580)	4.2 (610)
Poisson's Ratio	ν_{12} , (mm/mm)	0.32	0.12	0.58	0.31	-	0.12	0.58	0.31
<i>Equivalent Mechanical Properties of Flanges and Web of HFRP/GFRP I-Girders Obtained from Material Tests</i>									
HFRP I-Girder	Flanges			σ_{c11} N/mm ² (psi)	σ_{t11} N/mm ² (psi)	E_c kN/mm ² (ksi)			
	Web			394 (57,140)	884 (128,210)	49.4 (7,160)			
GFRP I-Girder	Flanges			-	449 (65,120)	20.2 (2,930)			
	Web			299 (43,370)	185 (26,830)	19.8 (2,870)			

Note: CSM = Continuous Strand Mat; subscripts “c” and “t” indicate compressive and tensile properties, respectively.

UHPFRC Slabs

Mix proportions of the UHPFRC slabs are listed in Table 2. The UHPFRC slabs were composed of ordinary Portland cement, silica fume, ettringite, sand, water, water-reducing agent, and steel fibers (Nguyen et al. 2013). The mix had a low water-to-binder ratio (about 14%), and the hardened UHPFRC may therefore be very dense. The UHPFRC is highly durable, with chloride ion ingress of about 10% that of ordinary concrete (Sakai and Noguchi 2013). The steel fibers had a diameter of 0.2 mm (0.008 in.) and a tensile strength of 2,000 MPa (290,280 psi). The fibers were 22 mm (0.87 in.) and 15 mm (0.59 in.) long, which may prevent them from bending during the concrete mixing. They were uniformly dispersed in the concrete in order to effectively resist cracks. The steel fibers also assisted in resisting shrinkage and temperature effects. The fibers were added at approximately 1.75% volume ratio with equal quantities of the 15 mm (0.59 in.) and the 22 mm (0.87 in.) lengths. The UHPFRC slabs were precast and cured for 48 hours (wet curing at 5-40°C (41-104°F) for the first 24 hours and steam cured at 85°C (185°F) for another 24 hours). Compression tests were performed on 100×200 mm (3.94×7.87 in.) UHPFRC cylinders to determine the compressive strength and modulus of elasticity. Three specimens were tested for each material property and the average values are listed in Table 3. The tensile modulus of elasticity (Young's modulus) of the UHPFRC is almost the same as its compressive modulus of elasticity.

Table 2 Mix Proportions of UHPFRC

Air content (%)	Unit quantity, kg/m ³ (lb/ft ³)				Steel fiber, kg (lb)
	Water	Pre-mixed cement	Sand	Water-reducing agent	
2.0	205 (12.6)	1,287 (79.4)	898 (55.4)	32.2 (2.0)	137.4 (1.75Vol %) (302.6)

Table 3 Mechanical Properties of UHPFRC, High-Strength Mortar, and Epoxy

Material	Compressive strength, N/mm ² (psi)	Modulus of elasticity, kN/mm ² (ksi)
UHPFRC	182 (26,420)	46.1 (6,690)
High-strength mortar	88.3 (12,820)	29.9 (4,340)
Epoxy	70-76 (10,160-11,030)	4-6.4 (580-930)

High-Strength Mortar and Epoxy

Mix proportions of the high-strength mortar are shown in Table 4. Mechanical properties of the mortar obtained from the material tests are listed in Table 3. A solvent free, high-strength, high-modulus, two-component epoxy (Sikadur-30) was used to connect the UHPFRC slabs to the HFRP girders and to connect every two adjacent UHPFRC segments. Table 3 shows compressive strength and modulus of elasticity of the epoxy. More detailed mechanical properties of the epoxy were presented by the authors elsewhere (Nguyen et al. 2012 and Nguyen et al. 2014).

Table 4 Mix Proportions of High-Strength Mortar

W/C (%)	Unit quantity, kg/m ³ (lb/ft ³)			
	Cement (C)	Water (W)	Fine aggregate	Air entraining and high-performance water-reducing agent
30	970.7 (59.9)	291.2 (18.0)	1026.9 (63.3)	9.7 (6.0)

FLEXURAL TEST SETUP AND VARIABLES

Four-point bending tests (Fig. 3) were conducted on nine large-scale girders. Cross-sectional dimensions and details of the FRP-UHPFRC composite girders are shown in Fig. 4 and Fig. 5, respectively. Loads were applied through a hydraulic jack until the failure of girders. The applied load, deflection at the mid-span section, and strains in the FRP-UHPFRC composite section were recorded throughout the test.

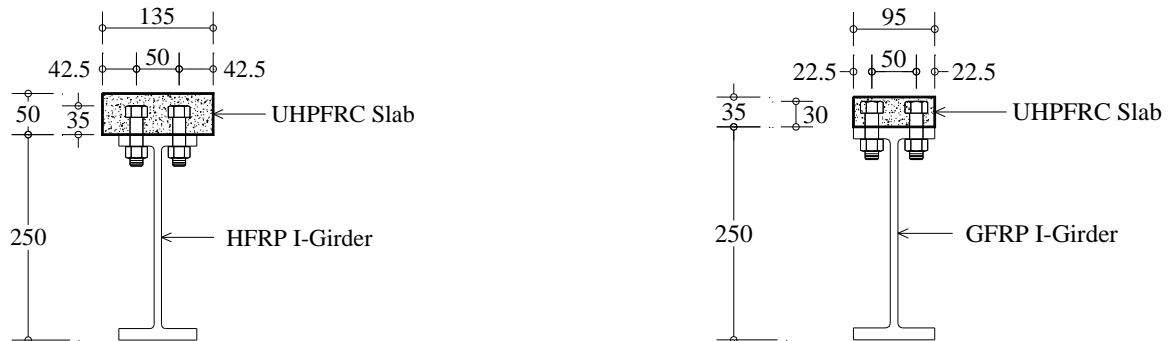
Two girder series were investigated: (1) H-series girders, including the HFRP I-girders topped with the precast UHPFRC slabs; and (2) G-series girders, which consist of the segmental UHPFRC slabs rested on the GFRP I-girders. UHPFRC slabs' width and thickness of H-series girders are 135 mm (5.31 in.) and 50 mm (1.97 in.), respectively, while those of the G-series girders are 95 mm (3.74 in.) and 35 mm (1.38 in.). Two types of precast UHPFRC slabs were evaluated, including full-length slabs and segmental slabs. The full-length slabs include a single precast UHPFRC segment with a length of 3,500 mm (137.8 in.) (Fig. 5a), while the segmental slabs (Fig. 5c-e) were made of twelve 300 mm (11.8 in.) long precast UHPFRC segments. The main test variables are the two types of FRP I-girder (i.e.

HFRP and GFRP girders), the UHPFRC slabs' dimensions, and the connection methods between the precast UHPFRC segments. Either epoxy or high-strength mortar was used to connect the segments of the segmental girders. For epoxy-connected girders, the epoxy was pre-applied to the segments and a gap between two successive segments was equivalent to the thickness of the epoxy layer (0.3-0.5 mm (0.012-0.02 in.)), as schematically shown in Fig. 6a. For mortar-connected girders, high-strength mortar was filled into the 10 mm (0.39 in.) gap between the adjacent segments after the segments were connected to the FRP girder by the epoxy. For G-series girders, two girders were strengthened with either CFRP or GFRP plate(s). CFRP plates (GM512) were provided by Mitsubishi plastics, Inc. Young's modulus and tensile strength of the CFRP plates were 156 GPa (22,630 ksi) and 2,400 MPa (348 ksi), respectively. The GFRP plates had a tensile strength of 500 MPa (72.5 ksi), while their Young's modulus was 25 GPa (3,630 ksi). The FRP plate(s) was externally bonded to the soffit of the FRP I-girder using the epoxy. The "off-the-self" thickness×width of the CFRP plates was 1.2×50 mm (0.047×1.97 in.) while the width and thickness of the GFRP plate was customized to be 95 mm (3.74 in.) and 8 mm (0.315 in.), respectively (Fig. 4c-d). It should be noted that two side-by-side CFRP plates were used to entirely cover the bottom flange of the FRP I-girder because the off-the-self width of the CFRP plates was about only half of the girder's flange width (Fig. 4c). On the other hand, the customized width of the GFRP plate was equal to that of the FRP girder's flange and a single GFRP plate was thus employed (Fig. 4d). The test variables of the FRP-UHPFRC composite girders are listed in Table 5.

The girder specimen identification scheme in Table 5 consists of three-part code as follows: *A-B-C*. Where *A* represents the girder type ("H" for the HFRP I-girder, "G" for the GFRP I-girder, "GC" for the GFRP I-girder strengthened with the CFRP plates, and "GG" for the GFRP I-girder strengthened with the GFRP plate); *B* designates the slab type ("FL" for the full-length precast slab, "SE" for the segmental precast slabs connected by the epoxy, and "SM" for the segmental precast slabs connected by the high-strength mortar); and *C* indicates the girders' loading span length ("LS7" for 700 mm (27.6 in.) loading span or "LS10" for 1,000 mm (39.4 in.) loading span).

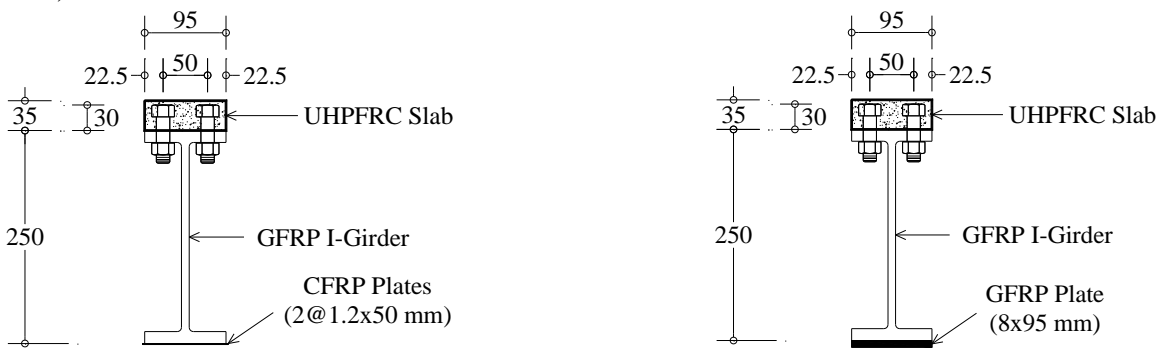


Fig. 3 Test setup of FRP-UHPFRC composite girders



a. H-series girders
(H-FL-LS10, H-SE-LS10, H-SE-LS7, and H-SM-LS7)

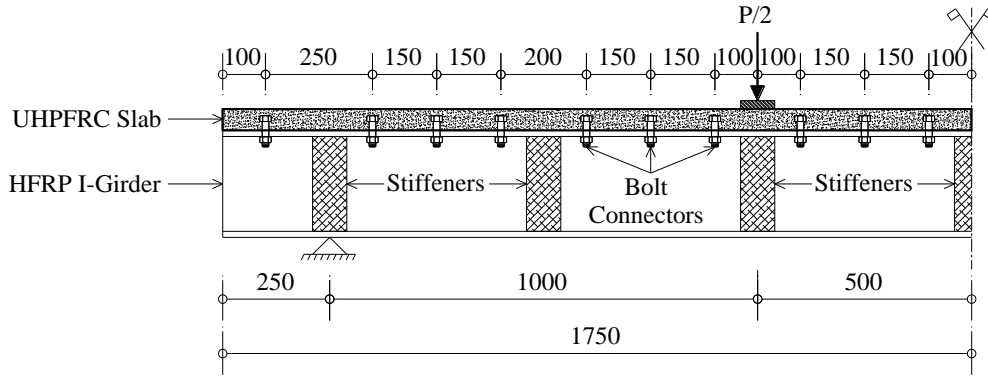
b. G-series girder (G-SM-LS7)



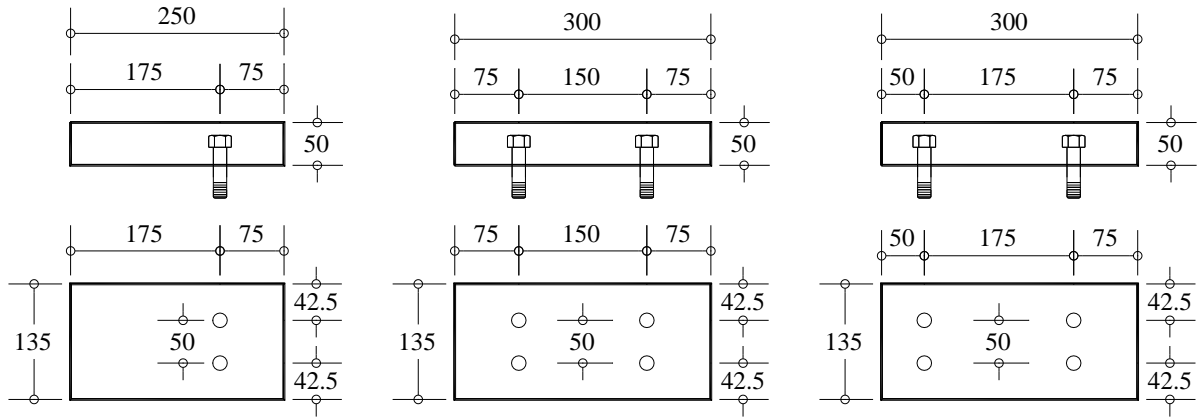
c. G-series girder (GC-SM-LS7)

d. G-series girder (GG-SM-LS7)

Fig. 4 Cross-sectional dimensions of FRP-UHPFRC composite girders (dimensions in millimeters)



a. Girder H-FL-LS10

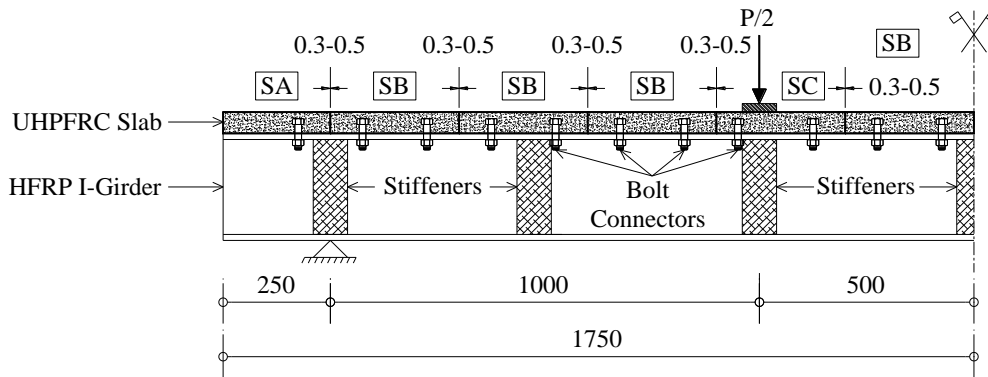


Segment A (SA)

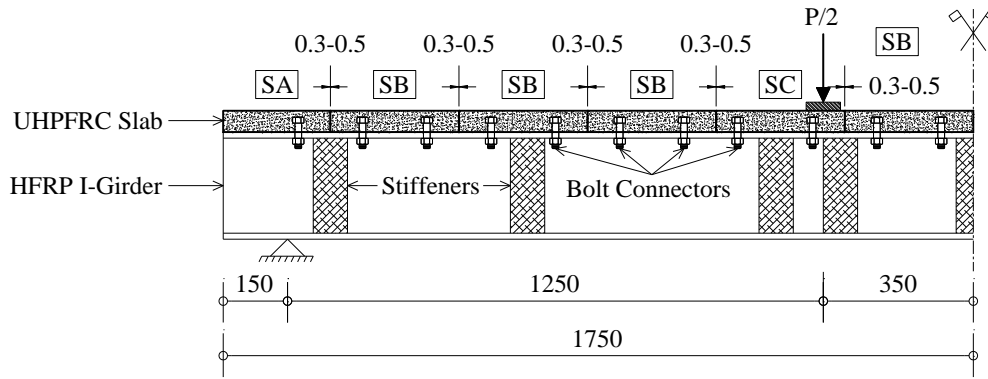
Segment B (SB)

Segment C (SC)

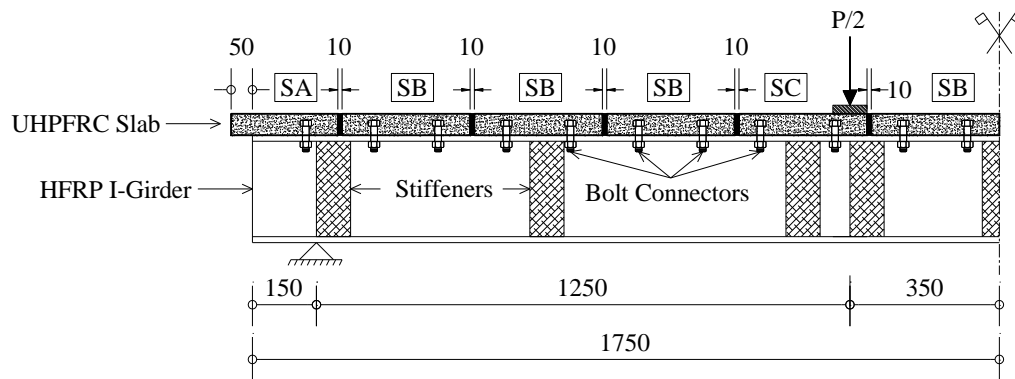
b. Precast UHPFRC segments used in girders H-SE-LS10, H-SE-LS7, H-SM-LS7, G-SM-LS7, GC-SM-LS7, and GG-SM-LS7



c. Girder H-SE-LS10



d. Girder H-SE-LS7



e. Girders H-SM-LS7, G-SM-LS7, GC-SM-LS7, and GG-SM-LS7

Fig. 5 Details of FRP-UHPFRC composite girders (dimensions in millimeters)



a. Epoxy-bonded connection



b. High-strength mortar connection

Fig. 6 Connection methods for UHPFRC segments

Table 5 Flexural Girder Test Variables

Specimen ID	FRP plate bonded to soffit of GFRP I-girder	FRP plate thickness, mm (in.)	Type of precast UHPFRC slab	UHPFRC slab width×thickness, mm (in.)	Type of connection between two adjacent UHPFRC segments	Gap between two adjacent UHPFRC segments, mm (in.)	Loading span length, mm (in.)
H-FL-LS10	—	—	Full-length	135×50 (5.31×1.97)	—	—	1,000 (39.37)
H-SE-LS10	—	—	Segmental	135×50 (5.31×1.97)	Epoxy	0.3–0.5 (0.012–0.02)	1,000 (39.37)
H-SE-LS7	—	—	Segmental	135×50 (5.31×1.97)	Epoxy	0.3–0.5 (0.012–0.02)	700 (27.56)
H-SM-LS7	—	—	Segmental	135×50 (5.31×1.97)	Mortar	10 (0.39)	700 (27.56)
G-SM-LS7	—	—	Segmental	95×35 (3.74×1.38)	Mortar	10 (0.39)	700 (27.56)
GC-SM-LS7	CFRP plates	1.2 (0.047)	Segmental	95×35 (3.74×1.38)	Mortar	10 (0.39)	700 (27.56)
GG-SM-LS7	GFRP plate	8.0 (0.315)	Segmental	95×35 (3.74×1.38)	Mortar	10 (0.39)	700 (27.56)
G-Control	—	—	—	—	—	—	700 (27.56)
H-Control	—	—	—	—	—	—	1,000 (39.37)

Note: G = GFRP I-girder; H = HFRP I-girder; FL = full-length precast slab; SE = segmental precast slabs connected by the epoxy; SM = segmental precast slabs connected by the high-strength mortar; LS10 = 1,000 mm (39.4 in.) loading span; LS7 = 700 mm (27.6 in.) loading span; G-Control = GFRP I-girder without slabs; H-Control = HFRP I-girder without slabs.

The authors have completed a comprehensive experimental program to investigate shear interaction between the FRP I-girders and the UHPFRC slabs. Fourteen push-out tests have been conducted and the results were reported by the authors elsewhere (Nguyen et al. 2014). The results showed that the combined use of epoxy and bolt shear connectors can effectively prevent slip between the FRP I-girders and the UHPFRC slabs. It can also greatly improve the shear strength of connectors and connection stiffness. The results of the push-out tests were used to design the large-scale FRP-UHPFRC composite girders. Bolt shear connectors and epoxy were used to connect the FRP girders to the UHPFRC slabs in all the tested

girders. High Corrosion Resistant Steel (HCRS) headed bolt shear connectors with 16 mm (0.63 in.) diameter were used. HCRS has powerful anti-rusting and anti-corrosive properties resulting from a superior fluorocarbon polymer treatment, and the HCRS shear connectors are considered to be very durable. The top flange surface of the FRP I-girders was roughened with sandpaper to increase the bond between the girder and the slab. All girders in this study were designed with full shear connection between the slab and the girder (i.e. designed number of bolt shear connectors was larger than that required for a full shear connection). Strains along section depth of the composite girders were monitored during the test. The strain gauge readings were used to examine the slip between the slab and the girder. The girders were designed to fail in tension and compression simultaneously. Details of the girders' cross-sections are shown in Fig. 4. The total length of each girder is 3,500 mm (137.8 in.), with the loading span being either 700 mm (27.56 in.) or 1,000 mm (39.37 in.) as shown in Fig. 5. Hollow GFRP box stiffeners with nominal dimensions of 30×60×220 mm (1.18×2.36×8.66 in.) and a wall thickness of 4 mm (0.16 in.) were bonded on both sides of the FRP I-girders by the epoxy to prevent buckling. Bolt spacing was varied based on locations of web stiffeners. A preset torque wrench was used to apply 20 N-m (14.74 lbf-ft) torque to the bolts.

FLEXURAL TEST RESULTS AND DISCUSSIONS

Comparisons of the load versus mid-span deflection curves of all the FRP-UHPFRC composite girders are shown in Fig. 7a. For comparison purposes, load-deflection curves of the control girders (GFRP and HFRP I-girders without UHPFRC slabs) are also included in Fig. 7a. The figure shows that both the control girders (G-Control and H-Control) behaved almost linearly up to the failure loads. The failure modes of these girders were crushing of fibers near the loading point followed by delamination of the compression flange and web crushing (Fig. 8a).

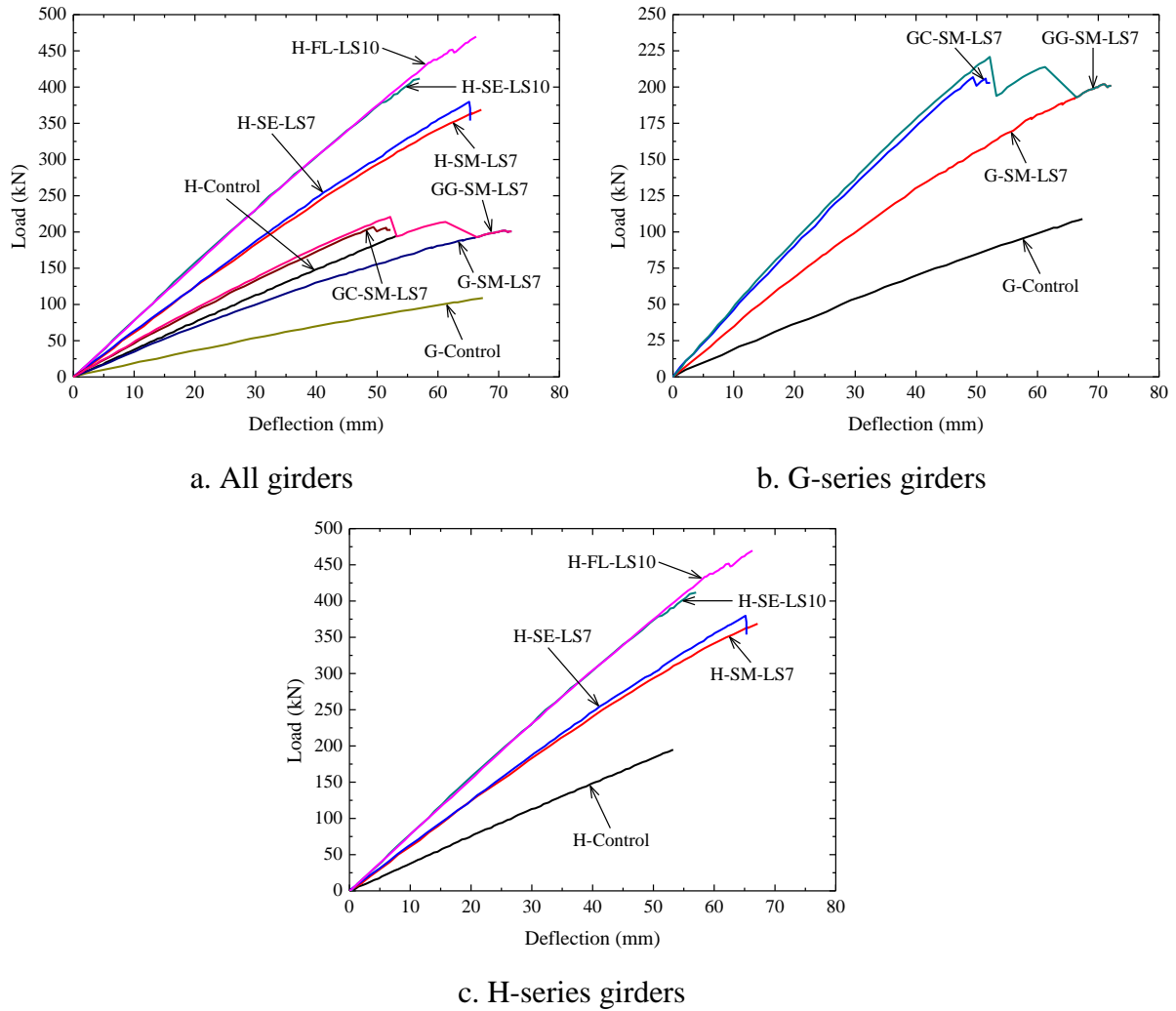


Fig. 7 Load versus deflection curves

It can be seen from Fig. 7a that the tested girders showed a brittle behavior up to the failure loads except girder GG-SM-LS7, which exhibited a pseudo-ductile behavior. This girder was strengthened with an 8 mm (0.31 in.) thick GFRP plate externally bonded to the soffit of the GFRP I-girder. Girder GG-SM-LS7 behaved almost linearly up to a load of 221 kN (49.6 kips). The load was then suddenly dropped to 194 kN (43.6 kips) due to the debonding of the GFRP plate. The girder continued carrying additional load after the second debonding at the load of 214 kN (48.1 kips), as shown in Fig. 7b. Girder GG-SM-LS7 is therefore considered to be pseudo-ductile as its stiffness reduction can give a warning of an imminent collapse. The results indicate that the epoxy bonding between the GFRP plate and the tension flange of the GFRP I-girder was quite satisfactory.

It is worth noting that girder GC-SM-LS7, which had two side-by-side 1.2 mm (0.047 in.) thick CFRP plates externally bonded to the soffit of the GFRP I-girder, exhibited a similar trend of the load-deflection curve as compared to girder GG-SM-LS7. However, girder GC-SM-LS7 failed shortly after the debonding of the CFRP plates due to crushing of the UHPFRC slab near the loading point, followed by fracturing of the GFRP I-girder and delamination at the CFRP/GFRP interface (Fig. 8b). This may be attributed to the high stress concentration at the CFRP/GFRP interface leading to total delamination between the CFRP plates and the GFRP tension flange. The stress concentration may be due to the mismatch in material properties between the CFRP plates and the GFRP girder's flange. In fact, Young's modulus of the CFRP plates is about 770% higher than that of the GFRP flange. On the other hand, there is only a 12% difference in Young's modulus between the GFRP plate and the GFRP flange; therefore, the stress concentration at the GFRP/GFRP interface of girder GG-SM-LS7 may be insignificant. It can be seen from Fig. 7b that the stiffness of girder GG-SM-LS7 at the last increment of the load-deflection curve was almost identical to that of girder G-SM-LS7 (without an epoxy-bonded plate). This result indicates that the GFRP plate can no longer carry additional load after the second debonding of girder GG-SM-LS7, and the load was carried solely by the UHPFRC slab and the GFRP I-girder, similar to girder G-SM-LS7.

Although both girders GG-SM-LS7 and G-SM-LS7 had a similar failure mode, which was concrete crushing of the UHPFRC slab followed by the fracture of the GFRP I-girder, the failure locations of these girders were different. Girder G-SM-LS7 failed near the mid-span section (Fig. 8c) while girder GG-SM-LS7 fractured near the loading point (Fig. 8d). In the case of girder GG-SM-LS7, this may be attributed to the bonded GFRP plate which led to the redistribution of stress in this girder after the debonding. Table 6 shows that the ultimate loads of girders GG-SM-LS7, GC-SM-LS7, and G-SM-LS7 are 2.03, 1.9, and 1.85 times higher, respectively, than that of the G-control girder without the UHPFRC slab. These results reveal that girder GG-SM-LS7 is more effective than the other G-series girders in terms of strength and ductility.



a. Girder G-Control



b. Girder GC-SM-LS7



c. Girder G-SM-LS7



d. Girder GG-SM-LS7



e. Girder H-SE-LS7



f. Girder H-SM-LS7

Fig. 8 Failure modes of FRP-UHPFRC composite girders with 700 mm (27.6 in.) loading span

Table 6 Summary of Girder Test Results

Specimen ID	P_u , kN (kips)	δ_u , mm (in.)	ϵ_{cu} (μ)	ϵ_{tu} (μ)	Failure mode
H-FL-LS10	469.7 (105.6)	66.3 (2.61)	4,290	10,970	Concrete crushing – UHPFRC slab (SS-LP); Delamination – HFRP top flange (SS-LP); Web crushing (SS-LP); Delamination – HFRP bottom flange (SS)
H-SE-LS10	411.7 (92.5)	57.0 (2.24)	3,140	9,400	Concrete crushing – UHPFRC slab (FS-LP); Delamination – HFRP top flange (FS-LP); Web crushing (FS-LP)
H-SE-LS7	379.7 (85.3)	65.2 (2.57)	3,440	10,960	Concrete crushing – UHPFRC slab (FS-LP); Delamination – HFRP top flange (FS-LP); Web crushing (FS-LP); Delamination – HFRP bottom flange (FS)
H-SM-LS7	368.7 (82.9)	67.2 (2.65)	2,210	10,860	Concrete crushing – UHPFRC slab (MS); Delamination – HFRP top flange (MS); Web crushing (MS); Delamination – HFRP bottom flange (FS); Mortar splitting
G-SM-LS7	201.9 (45.4)	71.1 (2.8)	3,060	11,070	Concrete crushing – UHPFRC slab (MS); Delamination – GFRP top flange (MS); Web crushing (MS); Mortar splitting
GC-SM-LS7	206.9 (46.5)	49.4 (1.9)	3,140	7,150	Concrete crushing – UHPFRC slab (SS-LP); Delamination – GFRP top flange (SS-LP); Web crushing (SS-LP); Delamination – CFRP plates (SS); Mortar splitting
GG-SM-LS7	220.8 (49.6)	52.2 (2.1)	3,000	8,410	Concrete crushing – UHPFRC slab (FS-LP); Delamination – GFRP top flange (FS-LP); Web crushing (FS-LP); Mortar splitting
H-Control	194.9 (43.8)	53.3 (2.1)	n/a	6,000	Delamination – HFRP top flange (SS-LP); Web crushing (SS-LP)
G-Control	108.9 (24.5)	67.4 (2.7)	n/a	7,490	Delamination – GFRP top flange (SS-LP); Web crushing (SS-LP)

FS = flexural span; SS = shear span; SS-LP = shear span – near the loading point; FS-LP = flexural span – near the loading point; MS = mid-span section; P_u = Ultimate load; δ_u = Deflection corresponding to the ultimate load; ϵ_{cu} = Ultimate compressive strain of the UHPFRC slab near mid-span section; ϵ_{tu} = Ultimate tensile strain of the FRP girder near mid-span section

For H-series girders, both girders H-FL-LS10 (with full-length slab) and H-SE-LS10 (with segmental slabs) behaved linearly and had a similar stiffness prior to debonding between the UHPFRC slabs and the HFRP I-girders. Stiffness reductions in girders H-SE-LS10 and H-FL-LS10 were observed at the loads of 380 kN (85.4 kips) and 430 kN (96.6 kips), respectively, as a result of debonding (Fig. 7c). The difference in debonding loads of these two girders were attributed to the difference in locations and spacing of bolt shear connectors

as shown in Fig. 5a and c. The load-carrying capacity of girder H-SE-LS10 is approximately 12% lower than that of girder H-FL-LS10. Girders H-FL-LS10 and H-SE-LS10 failed in similar failure modes, where crushing of the concrete near the loading point was followed by web crushing and delamination of the HFRP compression flange. Tensile failure of the HFRP bottom flange at the mid-span section was observed in girder H-FL-LS10, thus indicating that the high tensile strength of the CFRP laminae in the bottom flange was effectively utilized. The results show that girders H-SE-LS10 and H-FL-LS10 exhibited significantly higher stiffness and load-carrying capacities than those of the H-Control girder. The stiffness of the H-Control girder was about half that of girders H-SE-LS10 and H-FL-LS10. The load carrying capacities of these girders were 2.1 and 2.4 times higher, respectively, than that of the H-Control girder.

Figure 7c also shows comparisons of the load versus mid-span deflection curves for the two H-series girders with two different connection methods between the precast UHPFRC segments (namely epoxy-bonded connections and high-strength mortar connections as mentioned in the previous section). The stiffness of girder H-SE-LS7 (with epoxy-bonded connections) was almost the same as that of girder H-SM-LS7 (with high-strength mortar connections) for the load ranging from zero to approximately 150 kN (33.7 kips). When the load increased from 150 kN (33.7 kips) to failure, the stiffness of girder H-SE-LS7 was slightly higher than that of girder H-SM-LS7, which was attributed to progressive failure of the mortar connections. This result suggests that the stiffness reduction observed in girder H-SM-LS7 after the load of 150 kN (33.7 kips) makes it slightly more ductile than girder H-SE-LS7. Therefore, it may be a good idea to use mortar connections for the UHPFRC segments in order to overcome the brittle behavior of the HFRP-UHPFRC composite girders. Both girders H-SE-LS7 and H-SM-LS7 failed in similar failure modes, which were concrete crushing near the loading point, followed by web crushing and delamination of the compression flange (Fig. 8e-f).

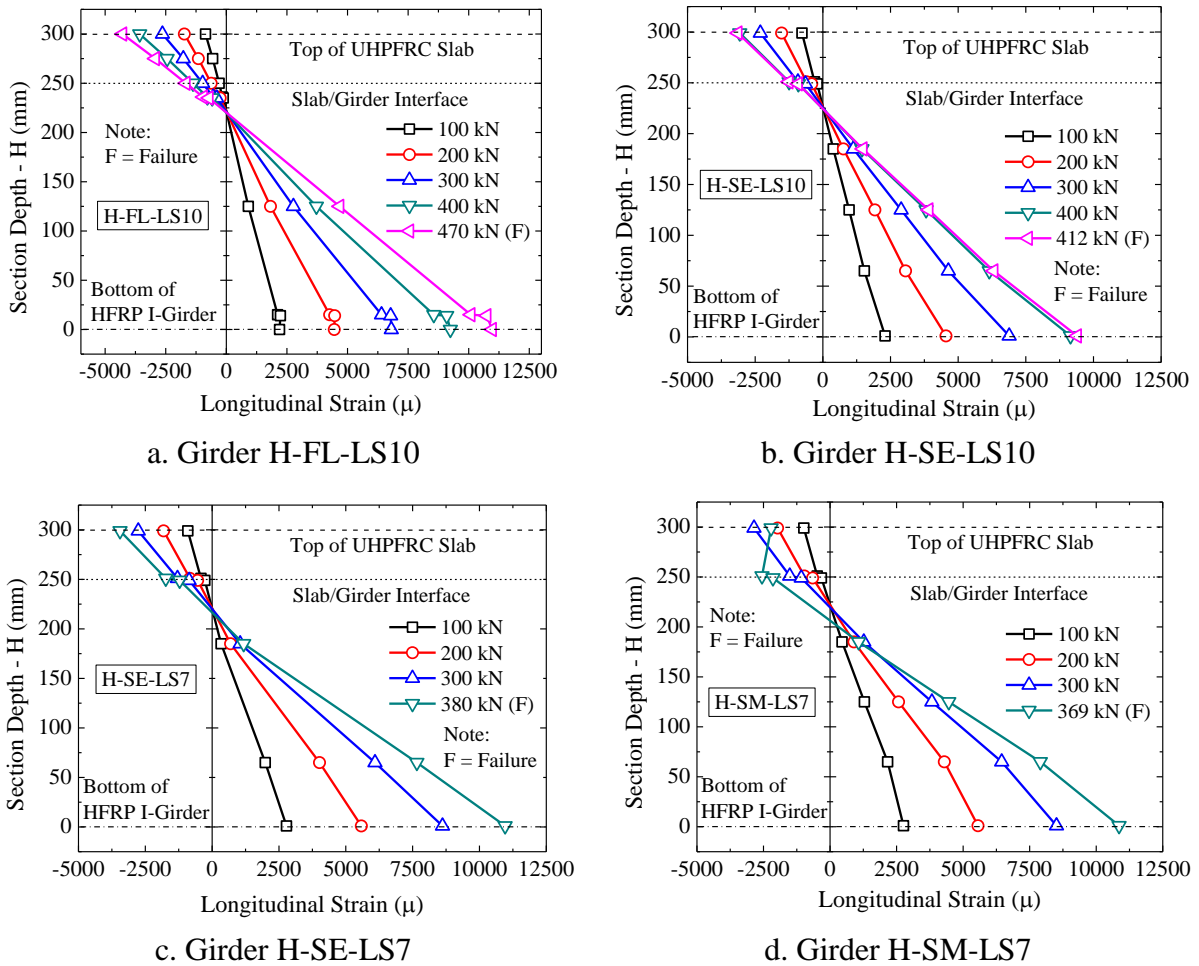


Fig. 9 Distribution of longitudinal strains along section depth of H-series girders near mid-span section

Figure 9 shows the distribution of longitudinal strains along section depth of the H-series girders near the mid-span section. Linear strain distributions through the cross-sections were, more or less, observed for girders H-FL-LS10, H-SE-LS10, and H-SE-LS7 (Fig. 9a-c). The results indicate that these girders exhibited almost a full interaction until the failure loads. On the other hand, curved strain distributions were observed through the cross-section of girder H-SM-LS7 (Fig. 9d). This may be attributed to progressive failure of the mortar connections. This girder failed due to mortar splitting and concrete crushing near the loading point, followed by web crushing and delamination of the compression flange (Fig. 8f).

The distribution of longitudinal strain along section depth of the G-series girders near the mid-span section was shown in Fig. 10. It should be emphasized that all the G-series girders

had the mortar connections between the precast UHPFRC segments. Similar to the H-series girder with the mortar connections (girder H-SM-LS7), curved strain distributions were observed through the cross sections of the G-series girders (Fig. 10a-c). Failure modes of these girders were almost identical to that of girder H-SM-LS7, which were mortar splitting and concrete crushing, followed by the fracture of the FRP I-girder.

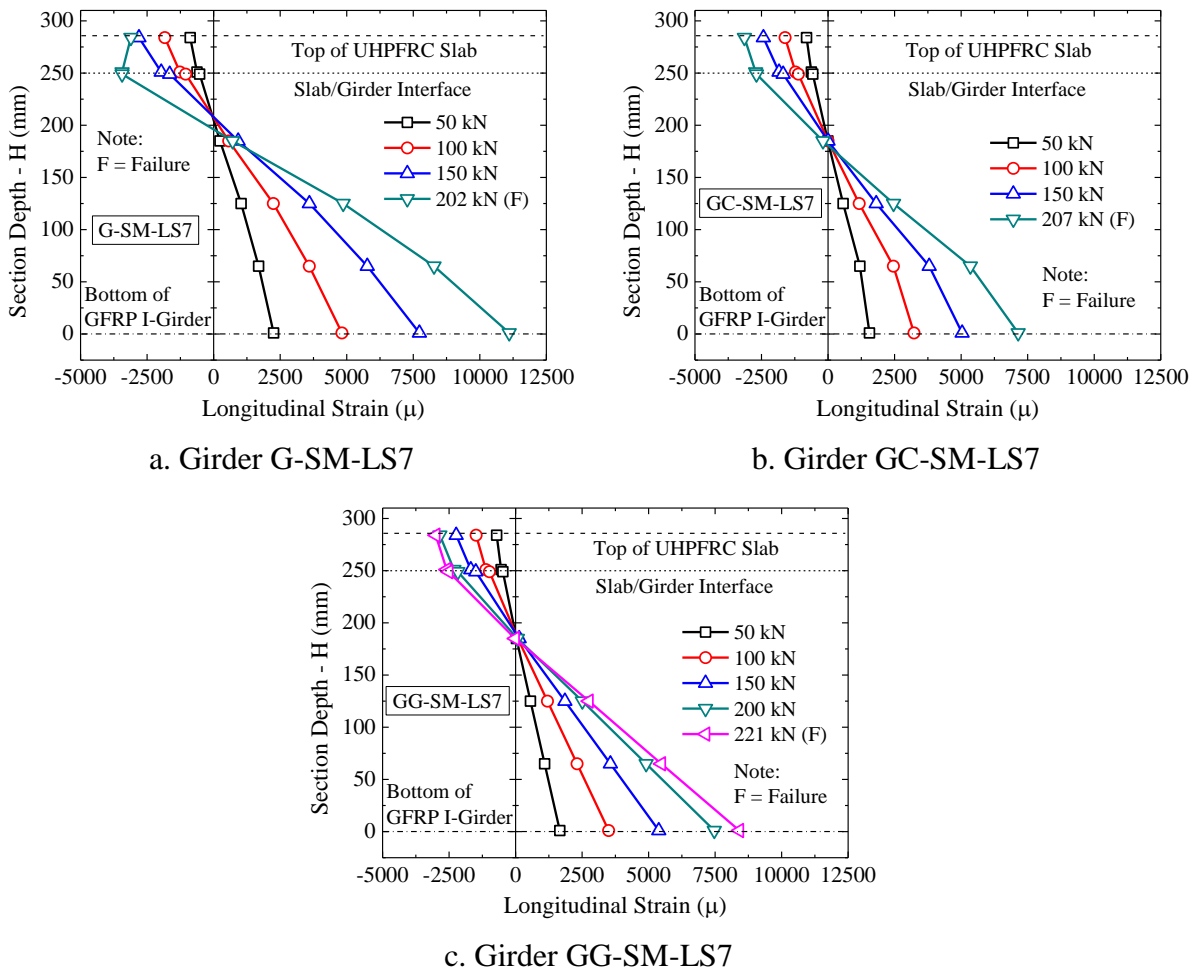


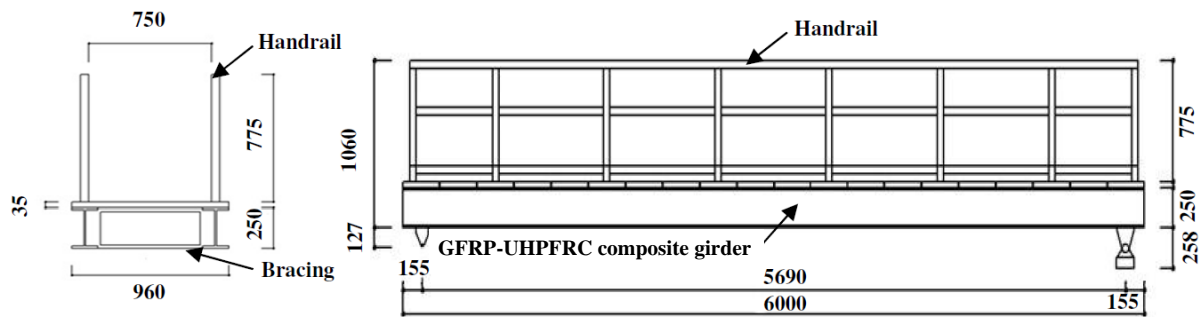
Fig. 10 Distribution of longitudinal strains along section depth of G-series girders near mid-span section

Maximum tensile strains recorded at the ultimate loads of H-series and G-series girders are approximately 10,970 μ and 11,070 μ, respectively. These strain levels are significantly higher than the tensile strains recorded at the ultimate loads of the H-Control and G-Control girders (Table 6). The results show that the addition of the UHPFRC slabs on top of the FRP

girders resulted in an effective utilization of the high tensile strength of the FRP materials. Summaries of all girder test results are listed in Table 6.

APPLICATION OF PRECAST FRP-UHPFRC COMPOSITE GIRDER SYSTEM TO AN ACTUAL PEDESTRIAN BRIDGE IN JAPAN

The applicability of the FRP-UHPFRC composite girder system has been proven by an actual pedestrian bridge, which was constructed in Onagawa town, Miyagi prefecture, Japan in 2012. The bridge was designed and constructed through a collaborative endeavor among universities, FRP manufacturers, industries, and local governments in Japan. The effective width and the overall length of the bridge were 750 mm (29.5 in.) and 6,000 mm (236.2 in.), respectively. The bridge was built with a segmental precast UHPFRC deck slab rested on two GFRP I-girders (Fig. 11a). The bridge was constructed in a fishing port, where chloride attack is an issue (Fig. 11b). Therefore, GFRP bolts were used in conjunction with epoxy adhesive to connect the GFRP I-girders and the UHPFRC slab. The use of the epoxy adhesive was verified by the authors to be very effective in obtaining a full interaction for the FRP-UHPFRC composite girders (Nguyen et al. 2015). The bridge was designed with a deflection limit of $L/500 = 12$ mm (0.47 in.), where L is the bridge's span length. The design live load of the bridge was 3.5 kN/m² (73 lbf/ft²). Further details of the GFRP-UHPFRC pedestrian bridge can be found elsewhere (METI Chubu and TAMA-TLO 2012, Wijayawardane et al. 2014, and Nguyen et al. 2015). Although the stiffness of this bridge is relatively low in comparison to conventional steel bridges, the FRP-UHPFRC girder system could provide a promising solution for short-span pedestrian/vehicular bridges, especially those are exposed to severe environmental conditions. In addition, the FRP I-girders and the UHPFRC slabs can be prefabricated in a factory and transported to the construction site. This results in rapid construction times, as was the case with the FRP-UHPFRC pedestrian bridge. The developed FRP-UHPFRC composite girder system is thus competitive and attractive for accelerated bridge construction.



(a) Details of GFRP-UHPFRC pedestrian bridge



(b) Completion of GFRP-UHPFRC pedestrian bridge connecting a pontoon and a concrete pier

Fig. 11 First GFRP-UHPFRC pedestrian bridge in fishing port in Onagawa, Miyagi, Japan (2012)

Summary of the construction cost of the HFRP pedestrian bridge in Kure, Hiroshima, Japan (Fig. 1) and the GFRP-UHPFRC bridge in Onagawa, Miyagi, Japan (Fig. 11) is shown in Table 7 (METI Chubu and TAMA-TLO 2012). Since these two bridges employed different girders' lengths and deck-girder systems, their construction costs are not comparable. The HFRP bridge included two HFRP I-girders topped with a GFRP grating deck while the GFRP-UHPFRC bridge composed of a segmental precast UHPFRC deck slab rested on two GFRP I-girders. For both bridges, it can be seen from Table 7 that the majority of the construction cost (about 90% on average) is the cost of materials. The average labor cost of the two bridges, which included the cost of assembly and installation, is approximately 10%

of the total cost. The HFRP bridge has a lower construction cost per unit area than the GFRP-UHPFRC bridge while it has a higher cost per unit weight.

Table 7 Construction Cost of HFRP and GFRP-UHPFRC Pedestrian Bridges

Bridge Girder System	Total Length, m (ft)	Effective Width, m (ft)	Total Weight, kg (lbs)	Material Cost (USD)	Labor Cost (USD)	Total Cost (USD)	Cost per Unit Area (USD per ft ²)	Cost per Unit Weight (USD per lbs)
HFRP	12.0 (39.4)	0.75 (2.46)	1,200 (2,646)	48,403	4,853	53,256	549	20.1
GFRP-UHPFRC	6.0 (19.7)	0.75 (2.46)	900 (1,984)	30,069	4,211	34,280	707	17.3

Note: The cost was converted from Japanese Yen (JPY) with an exchange rate of 1 USD = 123.5 JPY

CONCLUSIONS

This paper presents an experimental study of a sustainable composite girder system consisting of pultruded FRP I-girders and full-length/segmental precast UHPFRC topping slabs. High corrosion resistant steel (HCRS) headed bolt shear connectors and epoxy adhesive were used to connect the FRP I-girders and the UHPFRC slabs. The following main conclusions are drawn:

1. The H-series girders (HFRP I-girders topped with precast UHPFRC slabs) show much higher strength and stiffness than the G-series girders (precast UHPFRC slabs rested on GFRP I-girders). For the H-series girder with segmental slabs, the use of high-strength mortar connections for joining the precast UHPFRC segments may overcome the brittle behavior of the HFRP-UHPFRC composite girders. A stiffness reduction in the mortar-connected girders resulted from the progressive compressive failure of the high-strength mortar, which makes them slightly more ductile than the epoxy-connected girders.
2. The G-series girder with an 8 mm (0.315 in.) thick GFRP plate externally bonded to the soffit of the GFRP I-girder exhibits pseudo-ductile behavior and it is more effective than the other girders of the same series in terms of strength and ductility. On the other hand, the G-series girder strengthened with two side-by-side 1.2 mm (0.047 in.) thick CFRP plates shows more brittle behavior than the GFRP-plate-bonded girder due to delamination between the

CFRP plates and the GFRP tension flange. The delamination may result from the mismatch in material properties between CFRP and GFRP, leading to the relatively high stress concentration at the CFRP/GFRP interface.

3. The stiffness of the composite girder with the segmental precast slabs connected by epoxy was almost identical to that of the composite girder with the full-length precast slab. The ultimate strength of the segmental girder with epoxy connections was approximately 12% lower than that of the full-length precast girder, thus indicating a partial shear transfer across the epoxy connections.

4. Although design of the FRP-UHPFRC composite girders is governed by the stiffness and deflections of the girders (rather than their strength), the developed composite girders are promising for application to short-span pedestrian/vehicular bridges. These girders can also be used to rehabilitate existing structures and provide a competitive and sustainable option for accelerated bridge construction.

FUTURE WORKS

This study is limited to short-term monotonic behaviors of the FRP-UHPFRC composite girders. Long-term behaviors (for example, effects of ultraviolet degradation on FRP materials and impacts of temperature gradients, creep and shrinkage, cyclic loadings, etc.) and time-dependent dynamic behaviors of the FRP-UHPFRC composite girders should be investigated before recommending the developed girder system for real bridge applications.

ACKNOWLEDGMENTS

The authors gratefully acknowledge the financial supports from Japan Ministry of Economy, Trade, and Industry (METI) for this research project. We would like to thank the Kajima Corporation for providing the Ultra-High Performance Fiber-Reinforced Concrete as well as Fukui Fibertech Co., Ltd. and Toray Industries Inc. for providing the FRP materials. Gratitude is extended to Mr. Kensuke Shiroki and Mr. Tomoya Arai of the Structural Material Laboratory at Saitama University for their assistance in preparing and conducting the experiments.

REFERENCES

- ASCE (2013). Report Card for America's Infrastructure. *American Society of Civil Engineers*.
- Bakeri, P. A., and Sunder, S. S. Concepts for Hybrid FRP Bridge Deck Systems. *Serviceability and Durability of Construction Materials, Proceedings of the First Materials Engineering Congress*, Denver, Colorado, August 13-15, 1990, ASCE, Vol. 2, pp. 1006-1015.
- Correia, J. R., Branco, F. A., and Ferreira, J. G. Flexural Behaviour of GFRP-Concrete Hybrid Beams with Interconnection Slip." *Composite Structures*, Vol. 77, No. 1, 2007, pp. 66–78.
- Deskovic, N., Triantafillou, T. C., and Meier, U. Innovative Design of FRP Combined with Concrete: Short-Term Behavior. *Journal of Structural Engineering*, Vol. 121, No. 7, 1995, pp. 1069-1078.
- Fam, A. Z., and Rizkalla, S. H. Flexural Behavior of Concrete-Filled Fiber-Reinforced Polymer Circular Tubes. *Journal of Composites for Construction*, ASCE, Vol. 6, No. 2, 2002, pp. 123-132.
- Keller T., Schaumann E., Vallée T. Flexural Behavior of a Hybrid FRP and Lightweight Concrete Sandwich Bridge Deck. *Composites Part A*, Vol. 38, No. 3, 2007, pp. 879–889.
- METI Chubu and TAMA-TLO. Research and Development Report; 2012. In Japanese.
- Mutsuyoshi, H., Nguyen, H., Shiroki, K., Aravinthan, T., Manalo, A. Experimental Investigation of HFRP Composite Beams. *American Concrete Institute, ACI Special Publication 1 (275 SP)*, 2011, pp. 219-243.
- Nguyen, H., Mutsuyoshi, H., Asamoto, S., and Matsui, T. Structural Behavior of Hybrid FRP Composite I-Beam. *Journal of Construction and Building Materials*, Vol. 24, No. 6, 2010, pp. 956-969.
- Nguyen, H. and Mutsuyoshi, H. Structural Behavior of Double-Lap Joints of Steel Splice Plates Bolted/Bonded to Pultruded Hybrid CFRP/GFRP) Laminates. *Journal of Construction and Building Materials*, Vol. 30, 2012, pp. 347-359.
- Nguyen, H., Mutsuyoshi, H. and Zatar W. Flexural Behavior of Hybrid Composite Beams. *Transportation Research Record: Journal of Transportation Research Board, Structures 2013*, Vol. 2, No. 2332, 2013, pp. 53-63.

- Nguyen, H., Zatar, W., and Mutsuyoshi, H. Hybrid FRP Girders Topped with Segmental Precast Concrete Slabs for Accelerated Bridge Construction. *Transportation Research Record: Journal of Transportation Research Board*, Vol. 2, No. 2407, 2014, pp. 83-93.
- Nguyen, H., Mutsuyoshi, H., and Zatar, W. Push-Out Tests for Shear Connections between UHPFRC Slabs and FRP Girder. *Composite Structures*, Vol. 118, 2014, pp. 528-547.
- Nguyen, H., Mutsuyoshi, H., and Zatar, W. Hybrid FRP-UHPFRC Composite Girders: Part 1 – Experimental and Numerical Approach. *Composite Structures*, Vol. 125, 2015, pp. 631-652.
- Nguyen, H., Zatar, W., and Mutsuyoshi, H. Hybrid FRP-UHPFRC Composite Girders: Part 2 – Analytical Approach. *Composite Structures*, Vol. 125, 2015, pp. 653-671.
- Sakai, K., and Noguchi, T. (2013). *The Sustainable Use of Concrete*, CRC Press, Boca Raton, Florida.
- Sugano, S., Kimura, H., and Shirai, K. Study of New RC Structures Using Ultra-High-Strength Fiber-Reinforced Concrete (UFC) – The Challenge of Applying 200 MPa UFC to Earthquake Resistant Building Structures. *Journal of Advanced Concrete Technology*, Vol. 5, No. 2, 2007, pp. 133-147.
- Wijayawardane, I.S.K., Mutsuyoshi, H., Janaka, P.S.V.T., and Nguyen, H. FRP and Ultra-High Strength Concrete Slab Composite Girders for Accelerated Bridge Construction. *Proceeding of the 9th International Conference on Short and Medium Span Bridges*, Calgary, Alberta, Canada, July 15-18, 2014.